Effect of Wake Disturbance Frequency on the Secondary Flow Vortex Structure in a Turbine Blade Cascade

Christopher G. Murawski
Research Engineer,
Propulsion Directorate,
Air Force Research Laboratory, USAF,
Wright Patterson AFB, OH 45433

Kambiz Vafai
Professor, Fellow ASME,
Department of Mechanical Engineering,
The Ohio State University, Columbus, OH 43210

An experimental study of the effect of wake disturbance frequency on the secondary flow vortices in a two-dimensional linear cascade is presented. The flow Reynolds numbers, based on exit velocity and suction side surface length were 25,000, 50,000 and 85,000. Secondary flow was visualized by injecting smoke into the boundary layer and illuminating it with a laser light sheet located at the exit of the cascade. To simulate wakes from upstream blade rows, a set of spanwise cylinders were traversed across the front of the blade row. The flow visualization results with a single wake disturbance reveal that the recovery time of the secondary flow vortex structure decreases as the wake traverse velocity is increased. The results of flow visualization with multiple wakes showed that wake disturbance frequencies below the axial chord flow frequency allowed complete recovery of the secondary flow vortex structure before the next wake encounters the blade leading edge. Wake disturbance frequencies that exceeded the axial chord flow frequency resulted in no observable recovery of the secondary flow vortex structure. Axial chord flow frequency is defined as the axial velocity in the cascade divided by the axial chord length of the turbine blade. [S0098-2202(00)02203-3]

Introduction

The losses in a turbine stage may be divided into three categories: endwall secondary flow loss, profile loss, and end wall tip clearance loss (Sharma and Butler [1]). Secondary flow in a turbine passage is created by two mechanisms: the boundary layer interaction with the leading edge creates a horseshoe vortex, and streamwise vorticity is created in the blade passage from the momentum defect in the boundary layer as the flow turns through the blade passage. The vortices entrain the freestream flow and endwall boundary layer. As a result, secondary flow regions embody considerable momentum losses resulting in total pressure losses, which are detrimental to overall turbine efficiencies.

The development of secondary flow in a stationary linear turbine cascade was documented by Wang et al. [2] using still photography, smoke wires, and a laser light sheet. Their secondary flow vortex model accurately depicts the near endwall flow behavior in a stationary linear cascade. Similar flow behavior was observed in the present study, and shall be discussed later.

Low pressure turbine aerodynamics has received greater attention recently through efforts of Halstead [3], Murawski et al. [4], Qiu and Simon [5], Lake et al. [6], and Matsunuma et al. [7]. It is well established that for some low pressure turbine blades, that as the flow Reynolds number decrease to low levels the profile loss increases. In a study of annular cascade flow, Matsunuma et al. [7] found that as Reynolds numbers decrease, the endwall passage vortices increase in size, resulting in significantly higher secondary flow losses. Gregory-Smith et al. [8], utilizing a linear turbine cascade, also showed that as the endwall boundary layer thickness increases, which occurs as Reynolds numbers decrease, the passage vortices become broader.

Wake interaction occurs in the gas turbine engine environment due to the relative motion of the rotors and stators. Numerous experimental efforts have been conducted in which moving cylinders were placed upstream of test blades to study the effect of simulated wake interactions on midspan flow phenomena (Doorly [9], Dullenkopf et al. [10], Han et al. [11], and Halstead [12]). Using moving cylinders to study the details of unsteady wake disturbances on a downstream blade row has proven to be a valuable research tool, and we have employed a similar technique in our work.

Previous research efforts into unsteady wake disturbances on downstream blade rows have concentrated on the mid-span region of the turbine cascades. The research presented here will focus on the effects of wake disturbances on the secondary flow vortices in the endwall region of a turbine cascade. During wake passing events, four phenomena contribute to the disturbance of the secondary flow vortex structure. They are: the dynamic changes to the inlet flow angle as a result of the velocity deficit in the wake, the effect of the velocity deficit (negative jet) in the wake, elevated levels of turbulence in the wake, and wake disturbance frequency. The experimental effort presented in this paper will not address the quantitative distribution of these effects. The vortex structure will be affected by dynamic changes in the inlet flow angle. This will not result in the complete destruction of the vortex. Secondary flow vortices will exist in high freestream turbulence environments. However, during a wake passing event the temporary change in local turbulence level, as well as, the velocity deficit in the wake compound to destroy the secondary vortex structure. In the gas turbine engine, wakes from upstream stages are generated continuously. The frequency of these wakes will have an effect on the stability of the secondary vortex structures.

The purpose of this research is to investigate the effect of wake frequency on the secondary flow vortex structure. This research was conducted in a linear turbine cascade in order to study the flow field in greater detail than are possible in actual turbine engines. The flow Reynolds numbers were 25,000, 50,000, and 85,000. To visualize the three-dimensional vortices, the boundary layer flow was seeded with mineral oil smoke and illuminated by a laser sheet. The illuminated flow was recorded using a high-speed video camera at 200 frames per second.

Contributed by the Fluids Engineering Division for publication in the JOURNAL OF FLUIDS ENGINEERING. Manuscript received by the Fluids Engineering Division August 10, 1999; revised manuscript received March 27, 2000. Associate Technical Editor: D. Williams.

Experimental Method

Experimental Apparatus. A linear cascade was employed to study the low pressure turbine airfoil. A schematic of the test apparatus is provided in Fig. 1. Air is pulled through the apparatus by a 20 HP motor operating a centrifugal blower in the suction mode. Air flow through the test rig is controlled by a variable speed motor controller. The wind tunnel inlet bell-mouth directs the flow through a 53 cm square by 20 cm deep honeycomb flow straightener. The flow continues through a 7:1 converging nozzle to the 11.4 cm by 40.6 cm flow channel.

The cascade used in this experiment is illustrated in Fig. 2. It contains four geometrically identical, low pressure turbine blades with an axial chord length of 10.36 cm, and a span-to-chord length aspect ratio of 1.1. The suction surface length is 15.24 cm. The pitch-to-chord ratio (solidity) is 0.88 and the flow is turned through 95 deg. The three flow Reynolds number cases in this study were 25,000, 50,000, and 85,000. Reynolds number is based on exit flow velocity and suction side surface length.

The wake generator was designed to model an actual gas turbine engine blade passage. The wake generator contains a moving floor and ceiling shuttle into which cylinders are inserted. The wake generator assembly is traversed across the tunnel in the transverse direction. These wake generators traverse, remaining inline with the linear turbine cascade at all times. The cylinders are utilized to simulate the wakes generated by the vane row upstream of the blade rotor. The cylinders are located 6.35 cm upstream of the airfoil row. The wake generator cylinders are 9.5 mm diameter with a 91.7 mm pitch. The cylinders are driven across the flow path by a mechanism at velocities from 0.5 m/s to 5.0 m/s. The total translation distance was 38.1 cm. The velocity was sustained by driving a push bar with a 1 horsepower DC electric motor. The velocity history of the translation slide was recorded using a slotted bar and a photo-diode assembly.

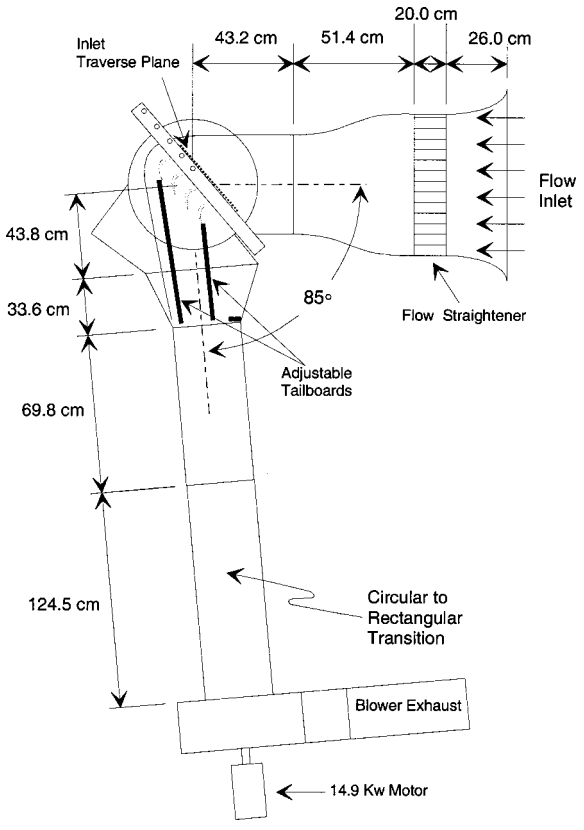

Fig. 1 Experimental setup

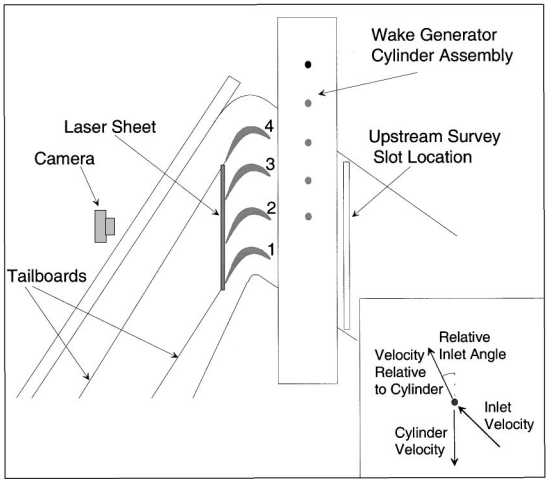

Fig. 2 Test section

Flow Visualization. The test section walls are constructed of clear plastic for visual access to the test section. Smoke was produced by an Aerolab smoke generator which vaporizes mineral oil. The smoke from the generator was injected into a 1.6 cm diameter copper tube located at the upper and lower edges of the inlet of the bellmouth. The smoke was ejected through fourteen 0.48 cm holes in the copper pipe. The smoke traveled into the bellmouth and remained within the boundary layer. This method of flow visualization has some advantages over the smoke wire method employed by Wang et al. [2] as the wires can create local turbulence in the flow field, while the method used in this study does not create extra turbulence. This method has the same limitation of requiring that the Reynolds number remain low in order to record clear video images. The beam from a 5 W ($Nd:YVO_4$) laser was expanded into a sheet to illuminate the flow, allowing imaging of the smoke laden vortices. The laser emitted a visible beam that was green (532 nm). The location of the laser sheet is illustrated in Fig. 2. When the wake generator was not used, video images were recorded at 30 frames per second using a Panasonic CCD camera with a 1:1.4 25 mm Electrophysics TV Lens, shutter speed of 1/500th of a second, and lens aperture of f1.4. When the wake generator was used, a high speed video system was required to capture the vortex-wake interaction. High speed video images were recorded at 200 frames per second using a NAC Inc. camera. The same lens was utilized, with a shutter speed of 1/2000th of a second, and an aperture of f2.6.

Instrumentation. Instantaneous local velocities were measured using a single element hot-wire probe. Mean inlet velocity and total pressure measurements were made using a pitot-static probe. The airfoil's surface static pressures were measured using 22 static pressure ports installed at midspan on the surface of one blade. The surface static pressure test blade was inserted in blade position 2 in the test section. One pressure tap is located near the front stagnation point, nine surface pressure taps are on the pressure side of the test blade and 12 static pressure taps are on the suction side of the test blade. The ports are connected to stainless steel tubing manifolded to a Scanivalve selector. Three different Validyne pressure transducers were used to cover the range of cascade pressures. Instrumentation output voltages were acquired using a National Instruments Data Acquisition Board. National Instruments LabVIEW software was utilized for data acquisition.

The experimental uncertainties were determined based on the method of Kline and McClintock [13]. The uncertainty of the velocity measurements resulting from pressure transducers and single wire, hot wire anemometer velocity measurements was calculated to be less than 2 percent. The maximum uncertainty in the pressure coefficient was calculated to be less than 4 percent.

Results

Inlet Velocity Profile. To verify an acceptable inlet flow, a velocity survey was performed using a single-element hot-wire probe. The survey was taken two blade chords upstream of the leading edges of the cascade blades at mid-tunnel height. The maximum variation from the mean inlet velocity was 3.57 percent, which occurred at a Reynolds number of 50,000. The average inlet freestream turbulence intensity was 0.61 percent.

Surface Static Pressure Surveys. Figure 3 illustrates the surface static pressure survey for the cascade at the Reynolds numbers used in this study. For all Reynolds numbers, the flow is attached for the whole length of the pressure side, which is the lower portion of the plot. The suction side is the top portion of Fig. 3. For all Reynolds numbers, the results show a separation occurring near 68 percent axial chord on the suction side. The largest boundary layer separation on the suction side was recorded for a Reynolds number of 25,000. As the Reynolds number is increased the point of flow reattachment moves forward, thus decreasing the size of the separation bubble. These results are similar to those reported by Murawski et al. [4] and Murawski and Vafai [14,15] in the same cascade used in this study, and Qui and Simon [5] and Lake et al. [6] in larger test rigs with the same blade goemetry.

Secondary Flow Symmetry. The linear cascade in this experimental study has a chord to height ratio of one. At low Reynolds numbers, large regions of secondary flow will exist. Figure 4 is an image of the secondary flow as it exits the cascade. A large vortex is seen in the corner of the endwall and suction side of each test blade. The vortices at the exit of the cascade have grown to dominate a large portion of the blade passage. A two-dimensional flow region is still present at the exit of the cascade on the centerline of each blade. The two-dimensional region is approximately 2.54 cm in height.

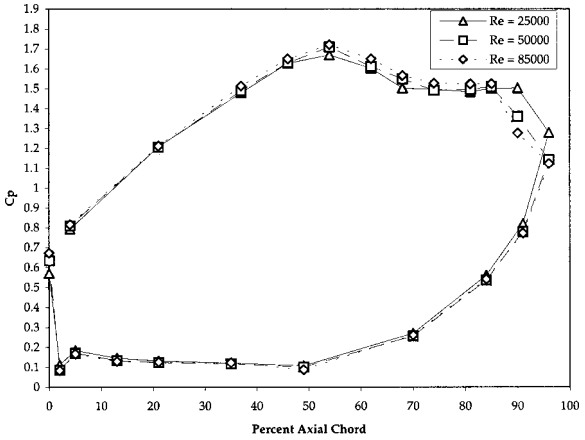

Fig. 3 Static pressure survey

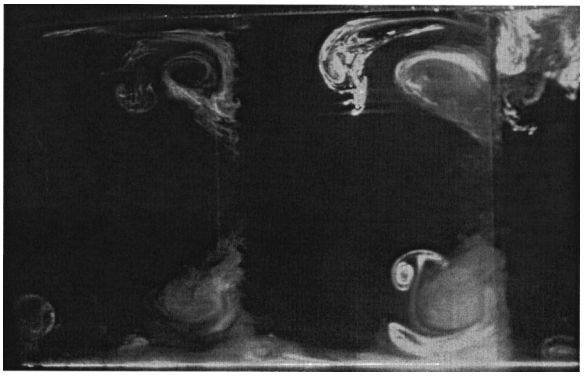

Fig. 4 Secondary flow vortex structure at the Cascade Exit Plane

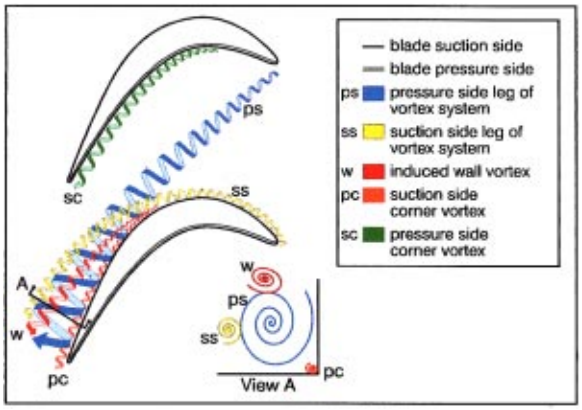

Fig. 5 Secondary flow vortex structure model

The behavior of the secondary flow seen in this study is very similar to that observed by Wang et al. [2]. In Fig. 4 the secondary flow vortex structure at the exit plane of the suction surface of the blade contains four vortices. Figure 5 is provided to explain the origin of these vortices in a linear turbine cascade. Figure 5 was created by applying the Wang et al. [2] flow model to our present results. The largest vortex is the passage vortex, which is created from the pressure side leg of the horseshoe vortex system. From the video it was seen that the passage vortex is very stable, and remained fixed in place. Two smaller vortices are wrapped around the passage vortex. Wang et al. [2] had shown that these vortices are the suction side leg of the horseshoe vortex and a wall vortex induced by the passage vortex. The fourth vortex is a small suction side corner vortex which is present in the corner of the endwall and the suction surface, under the larger multi-vortex structure.

Wake Generator Motion. Three configurations of the wake generator were tested. The first case was the wake generator operated without any rods in place to study the effect on the vortex structure of the moving shuttle without cylinders. The second case was the wake generator fitted with a single bar, to study the response of the secondary flow vortex structure to a single wake disturbance. The third case was the study of multiple wakes, with the intention to simulate the blade/wake interaction in real gas turbine engines.

Figure 6 illustrates typical velocity histories for each of the wake generator cases. Table 1 provides a summary of the wake generator characteristics. The wake generator assembly traverses from the pressure side toward the suction side of the blade set, moving across the front of the blade set from blade 4 toward blade 1. The wake generator assembly velocity was varied by setting the wake generator motor at 10 percent, 20 percent, 50 percent, and 80 percent of its maximum speed. The wake generator moves for 0.35 seconds for a motor setting of 10 percent, to 0.1 seconds for a motor setting of 80 percent. The high-speed video camera records at 200 frames per second, resulting in 70 frames for a motor setting of 10 percent and 20 frames for a motor setting of 80 percent. The wake generator assembly motion and the high speed video camera frame rate was more than adequate to record the reaction of the vortex structure to the flow disturbances.

Characteristics of Wakes From Cylinders. The wake generator assembly was traversed at different speeds which results in wakes with different characteristics. Table 2 presents the characteristics of the wakes from the wake generator cylinders. This experiment was conducted at three different Reynolds numbers

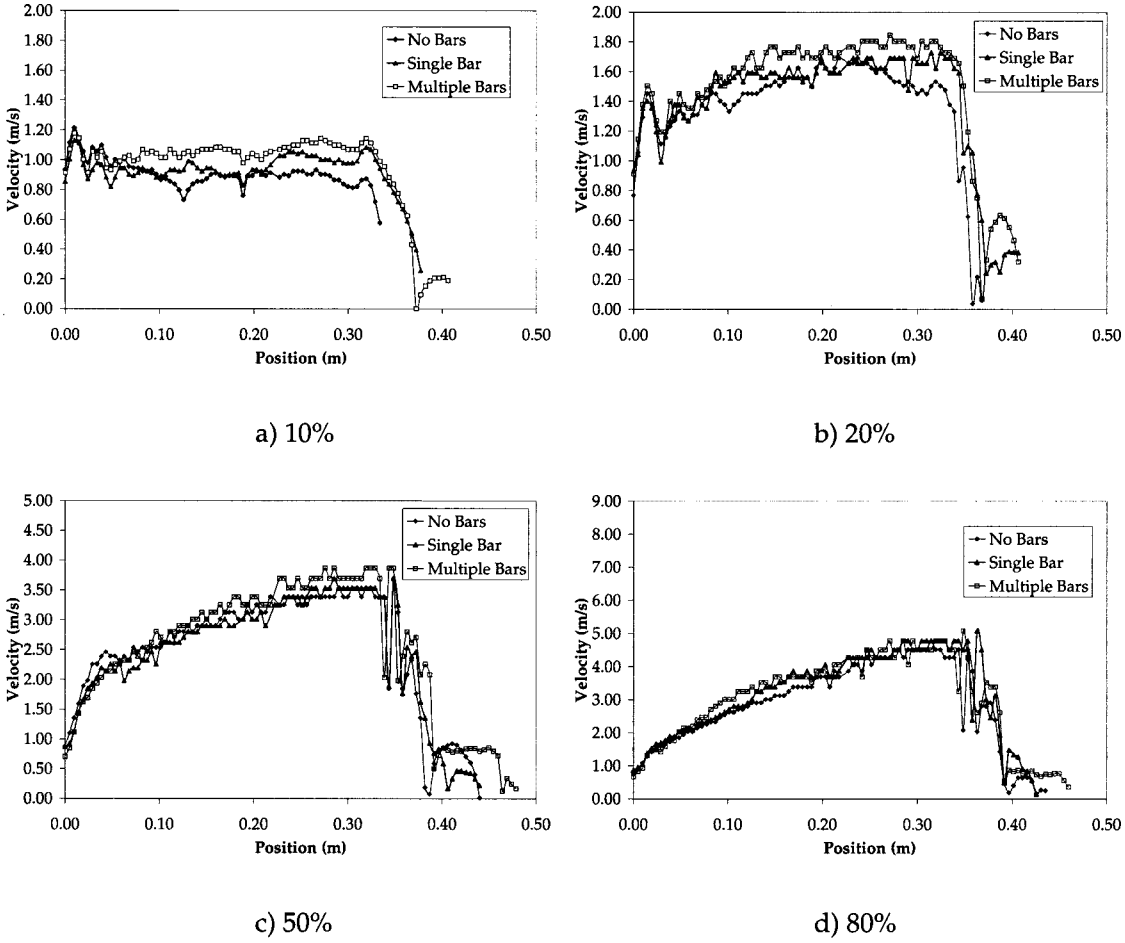

Fig. 6 Wake generator velocities with motor control set at (*a*) 10 percent, (*b*) 20 percent, (*c*) 50 percent, and (*d*) 80 percent

(25,000, 50,000, and 85,000) and four motor generator settings (10 percent, 20 percent, 50 percent, and 80 percent of total motor speed). The relative inlet angle of the wake approaching the blade set varies with changes in the flow Reynolds number and wake generator traversing velocity. At a steady inlet velocity, as the velocity of the wake generator cylinder increases the relative inlet angle of the wake approaching the blade goes down. For the case of Reynolds number of 25,000, the inlet angle varies by threefold from about 36 degrees at low wake generator speed (wake generator motor setting of 10 percent) to 13 degrees at the highest wake generator speeds (wake generator motor setting of 80 percent). At the higher Reynolds number case of 85,000, the change in inlet angle is about 5 to 3. The change in flow Reynolds number and relative inlet angle of the wakes has an effect on the wake/blade secondary flow interaction.

Table 1 Wake generator characteristics

Wake Generator Motor Setting	Wake Case	Steady State Velocity (m/s)	Frequency of Wakes (Hz)	Time at Constant Velocity (Sec)
10%	None	0.90	None	0.295
	Single	1.00	None	
	Multiple	1.07	11.66	
20%	None	1.59	None	0.110
	Single	1.69	None	
	Multiple	1.81	19.73	
50%	None	3.39	None	0.037
	Single	3.53	None	
	Multiple	3.69	40.23	
80%	None	4.51	None	0.021
	Single	4.78	None	
	Multiple	4.78	52.11	

Table 2 shows that the Reynolds numbers (based on relative velocity and cylinder diameter) from the wake generator cylinders remain below 9000. The relative velocity is the velocity the wake generator cylinder experiences by vector addition of the inlet flow velocity and motion of the wake generator. At these Reynolds numbers, the boundary layer on the wake generator cylinder is laminar and the boundary layer will separate at 80 degrees from the leading edge of the cylinder (Incropera and DeWitt [16]).

The characteristics of the wakes from the cylinders were not measured in this study. However, the cylinder wake characteristics should not differ from the result reported by Halstead et al. [12]. Halstead et al. [12] measured the wake characteristic of cylindrical rods and summarized their findings in several graphs which we will use to estimate wake width, total velocity deficit, peak turbulence intensity and turbulence intensity width. The width of the cylinder wake at the leading edge of the downstream blades was 1.905 cm. The total velocity deficit of about 25 percent, peak turbulence intensity in the cylinder wake of 14 percent, and turbulence intensity wake width of 3.096 cm.

Moving Wake Generator Cases

Moving Shuttle With No Wake Generators. Moving the shuttle with no wake generators was investigated to determine if a short duration moving floor segment ahead of the blade set would destroy the secondary vortex structure. In this case, the 50-cm wide shuttle moves in front of the blade set, from the suction side

Table 2 Characteristics of the wake generator cylinder

Wake Generator Motor Setting	Wake Case	Relative Inlet Angle (degrees)	Wake Generator Re #
Reynolds Number = 25000			
10%	None	35.99	None
	Single	34.56	2259
	Multiple	33.62	2309
20%	None	27.82	None
	Single	26.91	2829
	Multiple	25.88	2930
50%	None	17.11	None
	Single	16.60	4478
	Multiple	16.06	4625
80%	None	13.74	None
	Single	13.12	5734
	Multiple	13.12	5734
Reynolds Number = 50000			
10%	None	43.92	None
	Single	42.90	3759
	Multiple	42.20	3810
20%	None	37.62	None
	Single	36.83	4273
	Multiple	35.93	4361
50%	None	26.87	None
	Single	26.27	5775
	Multiple	25.61	5923
80%	None	22.66	None
	Single	21.83	6994
	Multiple	21.83	6994
Reynolds Number = 85000			
10%	None	48.04	None
	Single	47.35	5912
	Multiple	46.88	5965
20%	None	43.65	None
	Single	42.97	6390
	Multiple	42.27	6465
50%	None	34.60	None
	Single	34.04	7764
	Multiple	33.42	7904
80%	None	30.52	None
	Single	29.66	8937
	Multiple	29.66	8937

toward the pressure side of the blade. For all the flow cases the reaction of the secondary flow is similar. The moving wall segment in front of the blade set does not destroy the vortex structures. None of the vortices appear to change size during the duration of the shuttle movement. The passage vortex is pulled closer to the suction side. The vortices that ride on top of passage vortex are also pulled toward the suction surface. The suction side corner vortex remains intact and is also pulled toward the corner as the floor traverses across the front of the blade set. As the velocity of the traversing floor is increased, the vortices react in the same manner. The secondary flow vortices respond quicker as the speed of the shuttle is increased. The moving floor never destroys the secondary flow vortex system. However, the vortices respond more quickly to the increased speed of the flow disturbance.

Single Wake Disturbances. A single wake generator rod was traversed across the front of the blade passage to document the reaction and recovery behavior of the secondary flow vortex structure. The data collected in Table 3 were recorded using a constant source laser and a video camera with a 200 Hz frame rate. Images captured from the high speed video camera were not of sufficient quality for presentation in printed form. For illustrative purposes, clearer images were recorded using a pulsed laser and a digital camera with a frame rate of 30 Hz. Figure 7 presents the flow visualization results with one wake disturbance event using the pulsed laser. The flow behavior seen is exactly the same as that captured by the high frame rate camera. An undisturbed vortex structure is seen in Fig. 7(*a*) because the single wake generator has not been activated. The vortex structure is relatively stable

Table 3 Single wake vortex recovery results

Reynolds Number	Wake Generator Motor Setting (%)	Vortex Recovery Time (Sec.)
25000	10	0.08
	20	0.06
	50	0.04
	80	0.04
50000	10	0.06
	20	0.06
	50	0.05
	80	0.03
85000	10	0.02 – 0.025
	20	0.02 – 0.025
	50	0.02
	80	0.02

and similar to that seen in Fig. 4. Blade 2 is located at the center/right portion of Fig. 7. Blade 3, which is on the left side of Fig. 7, shows an undisturbed vortex structure in both images. In Fig. 7(*b*) the single wake generator cylinder is located upstream of Blade 2. At the left of Fig. 7(*b*), the vortex structure on blade 3 is intact. At the center/right portion of this image the single wake generator cylinder destroys the secondary flow structure.

A single wake disturbance is sufficient to temporarily disrupt the vortex structure. The vortex structure was disrupted in every case. Once the wake disturbance had passed, the secondary vortex structure re-establishes quickly. The disruption-to-recovery time recorded by the time-indexed high-speed video recorder varied with the wake generator motor speed and is presented in Table 3. This table shows that for the lower Reynolds number cases (25,000 and 50,000) the vortex recovery time is reduced by half

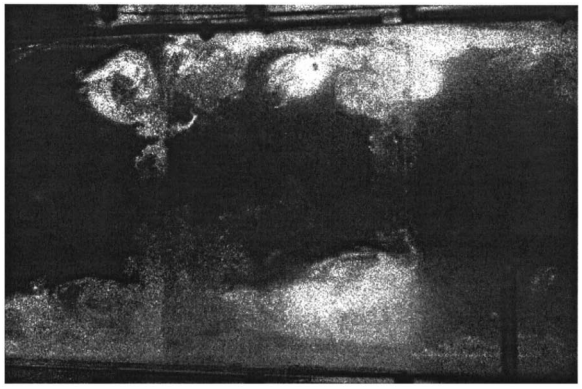

(*a*)

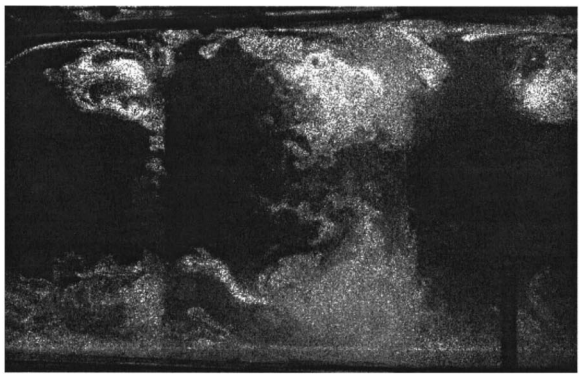

(*b*)

Fig. 7 Flow visualization with single wake passing event. (*a*) Undisturbed vortex structure; (*b*) one vortex structure intact and one vortex structure destroyed

when comparing the lowest (10 percent) and the highest (80 percent) wake generator motor settings. For a Reynolds number of 85,000, the vortex recovery time does not differ in each case. For the lower Reynolds number cases the vortex recovery time is affected by the large change in relative inlet angle and wake Reynolds number. Using Table 2 and Table 3, it is seen that the largest drop in vortex recovery time occurs when the relative inlet angle is halved. For example, at Reynolds number 25,000, the vortex recovery time (Table 3) significantly reduces from wake generator motor setting of 10 percent to 50 percent. However, when the Reynolds number is 85,000, the relative inlet angle only decreases by 40 percent from the lowest to highest wake generator motor setting, resulting in only a minimal change in vortex recovery time.

For the lower Reynolds number cases, it was shown that the time for vortex recovery decreased because the relative angle of the wake had decreased. Each wake of the wake generator cylinder may be viewed as a local region of highly turbulent, momentum deficient flow. Each blade cuts the wake as it interacts with the blade's leading edge, then each passage swallows a highly turbulent slug of wake flow. When the relative angle of the wake is decreased, the interaction time at the leading edge is decreased and the quantity of turbulent flow through the blade passage is also decreased. These factors result in a quicker vortex recovery time.

Figure 8 illustrates a single wake disruption of the vortex system in the linear cascade. The following sequence of wake and vortex interaction resulted from studying the high-speed video images. As the shuttle containing the single wake disturbance cylinder moves, the entire vortex structure reacts to the motion of the floor ahead of the blade set by migrating closer to the suction surface. The wake first strikes the pressure side of blade 3. The wake is cut by blade 3, at the same time the leading edge horseshoe vortex is destroyed. The cut wake begins to convect through the blade passage. When the wake encounters the suction side of blade 2, it disrupts the pressure side leg of the horseshoe vortex system. At the same time that this occurs, the leading edge of blade 2 will cut the wake, creating a highly turbulent slug that will move through the blade passage. The highly turbulent slug is too well mixed to contain coherent vortex structures. Before the wake contacts blade 2, the horseshoe vortex system on blade 3 has recovered from the single wake disturbance. Immediately following the wake, the passage vortex reappears briefly without the top riding pressure side leg of the horseshoe vortex system. Afterwards, three smaller vortices (wall vortex induced by the passage vortex, suction side leg of the horseshoe vortex system and suction side corner vortex) rejoin the passage vortex in a semi-stable system. It should be reiterated that this process occurs in a small window of time, from disruption to resurrection of the secondary flow vortex system.

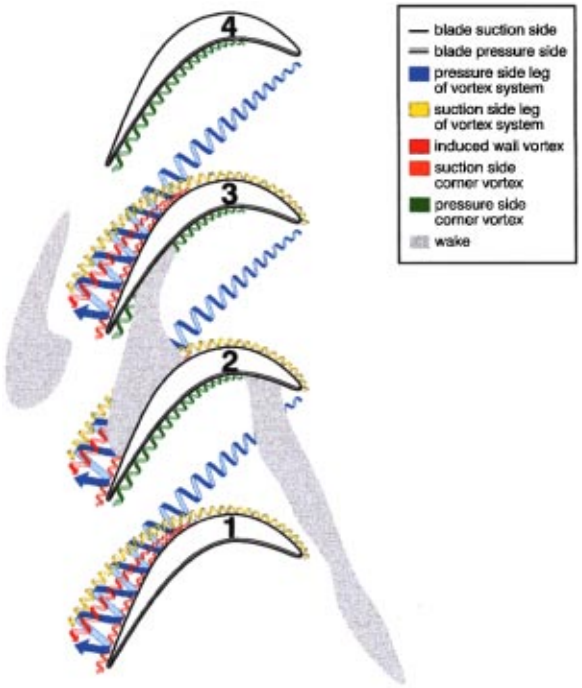

Fig. 8 Single wake flow model

Multiple Wake Disturbances. All the wake generator cylinders were installed to record the reaction of the secondary flow vortex structure with multiple wake disturbances. The observations in Table 4 were recorded by using a constant source laser sheet and a high speed (200 Hz frame rate) video camera. However, as in the previous section, the video images were not of sufficient quality to present in printed format. Therefore, for illustrative purposes, Fig. 9 presents the flow behavior for multiple wake passing events with images recorded using a pulsed laser and a digital camera (30 Hz frame rate). The flow behavior outlined in Fig. 9 is similar to the flow behavior seen on the high speed video. The disruption of the secondary flow vortex system is a very dynamic process. Figure 9(*a*) shows the undisturbed vortex structure, prior to the start of the wake generation. The wake generator moves from left to right in this figure. In Fig. 9(*b*) the multiple bar wake generator has entered the wind tunnel and is disturbing the vortex structure on blade 3 (left side of image), while the vortex structure from blade 2 (center/right side of image) remains intact. Fig. 9(*c*) shows the vortex structure has recovered on blade 3 as the wake generator has moved to a point midway between the cascade blades. The vortex structure is intact on blades 2 and 3. In Fig. 9(*d*), cylinders on the multiple bar wake generator have moved to a point in front of each cascade blade and results in the destruction of the vortex structure on both blades 2 and 3.

For each case the bar spacing is held constant. The velocity of the wake generator shuttle changes from case-to-case which results in a change in passing frequency of wake disturbance events. Referring to Table 1, as the velocity of the wake generator system increases the frequency of the wake increases. It should be noted that at a turbine blade flow Reynolds number of 50,000, the time for the flow to traverse the blade set in the axial direction is approximately 0.0382 seconds. This may also be restated as an axial chord flow frequency. The frequency of axial flow through the turbine blade cascade, is 26.2 Hz. The axial chord flow frequency (f_f) for each Reynolds number case is provided in Table 4.

Figure 10 illustrates the multiple wake passing results observed with the high speed video camera for a Reynolds number of 50,000. At the lowest wake generator motor setting (10 percent and 20 percent), it was observed that the vortex structure was disrupted by each wake passing event. However, the time between each wake passing event is long enough to enable the vortex

Table 4 Multiple wake vortex recovery results

Reynolds Number	Wake Generator Motor Setting (%)	Frequency of Wakes (f_w) (Hz)	$\frac{f_w}{f_f}$	Observation
25000 f_f=13.1 Hz	10	11.66	0.89	Recovery
	20	19.73	1.50	None
	50	40.23	3.07	None
	80	52.11	3.98	None
50000 f_f=26.2 Hz	10	11.66	0.45	Recovery
	20	19.73	0.75	Recovery
	50	40.23	1.53	None
	80	52.11	1.99	None
85000 f_f=44.5 Hz	10	11.66	0.26	Recovery
	20	19.73	0.44	Recovery
	50	40.23	0.90	Recovery
	80	52.11	1.17	None

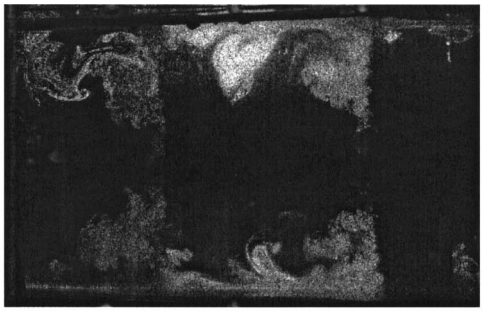

(*a*)

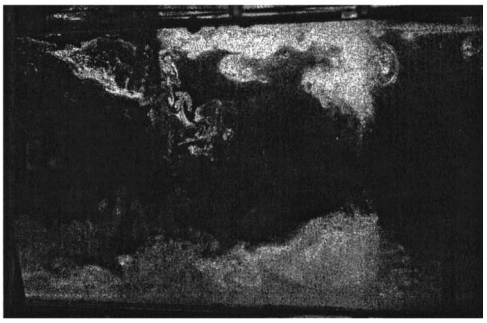

(*b*)

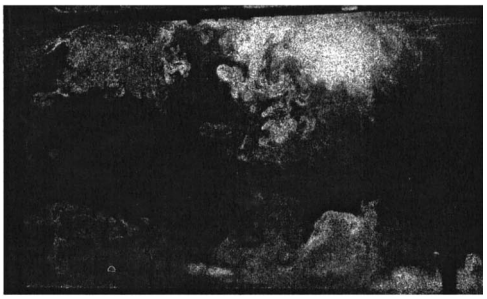

(*c*)

(*d*)

Fig. 9 Flow visualization with multiple wake passing events. (*a*) Undisturbed vortex structure; (*b*) One vortex structure destroyed and one vortex structure intact; (*c*) Upstream wakes about to destroy vortex structures; (*d*) Upstream wakes destroying both vortex structures

structure to recover (see Table 4). The vortex pattern was short lived, and was quickly disrupted by the next wake passing event. At higher wake generator motor speeds (wake generator motor setting of 50 percent and 80 percent), the interval between wake disturbance is so close that it will not allow the secondary flow vortex structure to regenerate.

The wake disturbance destroyed the vortex structure in a similar manner as seen in the single wake disturbance case. Once the wake passes the leading edge of the blade, the horseshoe vortex begins to regenerate. For the Reynolds number case of 50,000, the single wake passing disturbance case at 10 percent and 20 percent wake generator motor setting established that the vortex structure would reassert itself in 0.06 seconds (16.6 Hz). As seen in Table 4, the 10 percent and 20 percent wake generator motor setting case for multiple wakes established wake frequency of about 11.66 and 19.73 wakes per second, respectively. Since the time between wakes in the 20 percent case is less than the single wake vortex reestablishment time of 0.06 seconds, we may conclude that vortex recovery time is not as important as the ratio of wake disturbance frequency to axial chord flow frequency. For both low wake generator motor setting cases the frequency of the wakes was below the axial chord flow frequency of 26.2 Hz. The secondary flow vortex system is able to reestablish and grow through the blade passage before the next wake hits the blade leading edge.

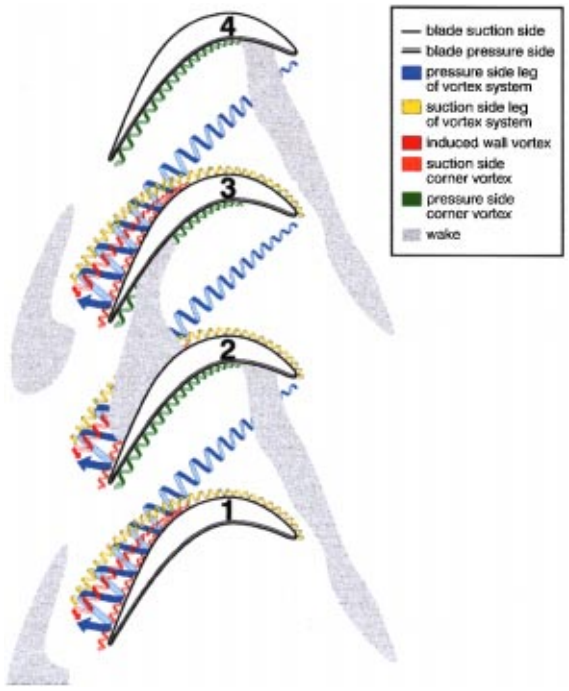

Fig. 10 Multiple wake with vortex recovery flow model

For Reynolds number of 50,000 and wake generator motor settings of 50 percent and 80 percent of the maximum power, there was no visible recovery of the secondary flow vortex structure at the exit of the blade passage. Table 4 shows that the wake disturbance frequency for the wake generator motor setting of 50 percent and 80 percent was 40.23 Hz and 52.11 Hz, respectively. These wake frequencies exceed the turbine axial chord flow frequency of 26.2 Hz. There is not sufficient time between wake passing disturbances to allow for the recovery of the secondary flow vortex structure in the blade passage.

Table 4 shows that the trend described above is valid for the other Reynolds numbers. The vortex structure only recovers when the frequency of the wake disturbances are below the axial chord flow frequency.

Conclusions

The present study investigated the reaction of the secondary flow vortex structure in a turbine cascade with variable wake frequency. Reynolds number was varied from 25,000, 50,000, and 85,000. The secondary vortex structure recorded in this study was compatible with established secondary flow theory. Cylinders

were traversed across the front of the blade row to simulate turbine blade disturbances. The velocity of the wake generator assembly was varied from 1.0 m/s to 4.8 m/s. The high-speed camera, with a frame rate of 200 frames per second, proved adequate to visualize the reaction of the vortex structure to the flow disturbances.

The flow visualization was carried out for three different cases.

First, the movement of the wake generator shuttle with no wake generators was investigated. The short duration shuttle motion without wake generators did not destroy the secondary flow structure. In each case, vortices remained intact and were temporarily pulled to the pressure side of the turbine blade. The vortex structure returned to its original configuration when the wake generator shuttle stopped moving. The vortices respond quicker, but in a similar manner, as the shuttle speed was increased.

Next, a single wake generator rod was placed in the shuttle and traversed across the front of the blade set at various velocities. The single wake disturbance temporarily disrupted the vortex structure. When the relative inlet angle of the wake was decreased by half, from the low to high speed wake generator assembly cases, the vortex recovery times were decreased by half. The higher wake generator velocity resulted in a decreased relative inlet angle and a decreased quantity of higher turbulence wake flow through the blade passage. It was observed that the secondary vortex structure began to recover even while a neighboring blade is immersed in a wake disturbance event.

Finally, all the wake generators were installed and run at varied velocities. The space between the wake generator cylinders was kept constant which created wake disturbance frequencies from 12 Hz to 52 Hz. It is shown that to sustain the destruction of the secondary flow vortex structure, the wake disturbance frequency must exceed the axial chord flow frequency. When the wake disturbance frequency is below the axial chord flow frequency, the secondary flow vortex structure is able to re-establish itself between each wake disturbance event.

The ratio of wake passing frequency to axial chord flow frequency in a gas turbine engine will be dependent on the number of blades, rotational speed, and the mass flow through the engine. Secondary flows create the second greatest profile losses in the high-pressure turbine stage (film cooling losses are the greatest). Low-pressure turbines contain blades with larger aspect ratios, therefore the secondary flows have a lesser affect on total profile losses. If these vortices are attenuated, the resulting reduction in total pressure loss will result in improved stage performance. Most high-pressure turbine stages will have a ratio of wake passing frequency to axial chord flow frequency greater than 1, therefore the secondary flow vortex structure will not recover between wake disturbances. In the low-pressure turbine, at certain design points, the secondary flow vortex structure will recover between wake disturbance events.

Acknowledgments

The authors are grateful for the assistance from members of the Air Force Research Laboratory Basic Aerothermal Research Program and the support of Dr. Paul King of the AFIT Aeronautical Engineering Department for use of the linear cascade. The authors would also like to acknowledge the technical and financial support provided by the Turbine Branch of the Air Force Research Laboratory's Propulsion Directorate.

Nomenclature

Cp = local pressure coefficient $((P_{Tin}-P_{Si})/\frac{1}{2}\rho U_{\mathrm{OUT}}^2)$
d = wake generator cylinder diameter
f_f = axial chord flow frequency
f_w = wake disturbance frequency
P_{Si} = static pressure along the blade surface
P_{Tin} = total pressure at inlet of the blade set
Re = Reynolds number $(U_{\mathrm{OUT}}(\mathrm{SSL})/v)$
SSL = suction surface length
Tu = freestream turbulence intensity $(u'_{\mathrm{rms}}/\overline{u}_{\mathrm{local}})$
U_{OUT} = average velocity out of the blade set
u'_{rms} = root mean square of fluctuating component of streamwise velocity
$\overline{u}_{\mathrm{local}}$ = local mean streamwise velocity
x = distance downstream from cylinder
v = kinematic viscosity
ρ = density

References

[1] Sharma, O. P., and Butler, T. L., 1987, ''Prediction of Endwall Losses and Secondary Flows in Axial Flow Turbine Cascades,'' ASME J. Turbomach., **109**, pp. 229–236.
[2] Wang, H.-P., Olson, S. J., Goldstein, R. J., and Eckert E. R. G., 1995, ''Flow Visualization in a Linear Turbine Cascade of High Performance Turbine Blades,'' ASME Paper No. 95-GT-7.
[3] Halstead, D. E., 1996, ''Boundary Layer Development in Multi-Stage Low Pressure Turbines,'' Ph.D. dissertation, Iowa State University.
[4] Murawski, C. G., Sondergaard, R., Rivir, R. B., Vafai, K., Simon, T. W., and Volino, R. J., 1997, ''Experimental Study of the Unsteady Aerodynamics in a Linear Cascade with Low Reynolds Number Low Pressure Turbine Blades,'' ASME Paper No. 97-GT-95.
[5] Qui, S., and Simon, T. W., 1997, ''An Experimental Investigation of Transition as Applied to Low Pressure Turbine Suction Surface Flows,'' ASME Paper No. 97-GT-455.
[6] Lake, J. P., King, P. I., and Rivir, R. B., 1999, ''Reduction of Separation Losses on a Turbine Blade with Low Reynolds Number,'' AIAA Paper No. 99-0242.
[7] Matsunuma, T., Abe, H, and Tsutsui, Y., 1999, ''Influence of Turbine Intensity on Annular Turbine Stator Aerodynamics at Low Reynolds Numbers,'' ASME Paper No. 99-GT-151.
[8] Gregory-Smith, D.G., Graves, C. P., and Walsh, J. A., 1988, ''Growth of Secondary Losses and Vorticity in an Axial Turbine Cascade,'' ASME J. Turbomach., **110**, pp. 1–8.
[9] Doorly, D. J., 1988, ''Modeling the Unsteady Flow in a Turbine Rotor Passage,'' ASME J. Turbomach., **110**, pp. 27–37.
[10] Dullenkopf, K., Shulz, A., and Wittig, S., 1991, ''The Effect of Incident Wake Conditions on the Mean Heat Transfer on an Airfoil,'' ASME J. Turbomach., **113**, pp. 412–418.
[11] Han, J.-C., Zhang, L., and Ou, S., 1993, ''Influence of Unsteady Wake on Heat Transfer Coefficient From a Gas Turbine Blade,'' ASME J. Heat Transfer, **115**, pp. 104–115.
[12] Halstead, D. E., Wisler, D. C., Okiishi, T. H., Walker, G. J., Hodson, H. P., and Shin, H.-W., 1995, ''Boundary Layer Development in Axial Compressors and Turbines Part 4 of 4: Computations and Analysis,'' ASME Paper No. 95-GT464.
[13] Kline, S. J., and McClintock, F. A., 1953, ''Describing Uncertainties in Single-Sample Experiments,'' Mech. Eng. (Am. Soc. Mech. Eng.), **75**, pp. 3–8.
[14] Murawski, C. G., and Vafai, K., 1999, ''Effect of Variable Axial Chord on a Low Pressure Turbine Blade,'' AIAA J. Propulsion and Power, **15**, pp. 667–674.
[15] Murawski, C. G., and Vafai, K., 2000, ''An Experimental Investigation of the Effect of Freestream Turbulence on the Wake of a Separated Low-Pressure Turbine Blade at Low Reynolds Numbers,'' ASME J. Fluids Engineering, **122**, pp. 431–433.
[16] Incropera, F. W., and DeWitt, D. P., 1985, *Fundamentals of Heat and Mass Transfer*, 2nd ed., Wiley, New York.